Honda Research Institute EU
Honda Research Institute Europe GmbH
https://www.honda-ri.de/

Automatic differentiation-based level set topology optimization for noise minimization in 3D domains considering acoustic-structure interaction

Andreas Neofytou, Thiago de Jesus de Araujo Rios, Mariusz Bujny, Stefan Menzel, Hyunsun Alicia Kim

2025

Preprint:

This is a post-peer-review, pre-copyedit version of an article published in Structural and Multidisciplinary Optimization. The final authenticated version is available online at: https://doi.org/10.1007/s00158-025-03995-z

Structural and Multidisciplinary Optimization (2025) 68:67
https://doi.org/10.1007/s00158-025-03995-z

INDUSTRIAL APPLICATION PAPER

Automatic differentiation-based level-set topology optimization for noise minimization in 3D domains considering acoustic-structure interaction

Andreas Neofytou[1] · **Thiago Rios**[2] · **Mariusz Bujny**[3] · **Stefan Menzel**[2] · **H. Alicia Kim**[1]

Received: 9 June 2024 / Revised: 27 December 2024 / Accepted: 9 March 2025
© The Author(s), under exclusive licence to Springer-Verlag GmbH Germany, part of Springer Nature 2025

Abstract
The reduction of vehicle interior noise is an important consideration in vehicle design and has become an active research topic in recent years. In this paper, we propose a modularized level-set topology optimization (mLSTO) methodology to address noise minimization. One of the main aims of this work is to enable more design freedom compared to previous works in which only size parameters are optimized. In addition, compared to previous topology optimization (TO) works for noise reduction, we also include structural capability by imposing stress constraints in combination with the noise reduction objective. We illustrate the applicability of the methodology by solving a one-way coupled vibro-acoustic optimization problem in a simplified 3D vehicle cabin. The main objective is to minimize the noise perceived at specified locations in the cabin due to vibrations of a range of frequencies. Our proposed mLSTO method employs a boundary perturbation scheme that allows for the use of automatic differentiation (AD) to compute the design sensitivities. The value of our automated approach is its generality. It can be straightforwardly adapted to more complex physical modeling and to completely different types of problems. Here, we demonstrate the noise reduction capability of the method by designing the vehicle cabin floor. Designs for different frequencies are obtained under a volume and stress constraints. The optimized designs indicate significant reductions in the noise compared to the baseline design and with additional material reductions.

Keywords Level-set topology optimization · 3D vibro-acoustics · Cabin noise reduction · Concept design

1 Introduction

The importance of noise, vibration, and harshness (NVH) performance has increased in the automotive and aircraft industries, and a variety of practical noise reduction methods have been proposed. In particular, reducing interior noise is considered a crucial target for passenger comfort in applications such as urban air mobility (Johnson and Silva 2018). Considering acoustic criteria is, thus, important already at the early stages of the development process. In this work, we propose a topology optimization (TO) method for designing parts of the vehicle body to reduce noise generated by vibro-acoustic interaction. Mechanical vibrations generated by the various components of a vehicle such as the powertrain and the interaction with the road cause noise in the cabin which leads to discomfort of the occupants. Hence, a design requirement of growing interest is to reduce the acoustic sound pressure level (SPL), measured in decibels (dB). The SPL is a widely accepted and well-established

Responsible editor: Axel Schumacher

✉ Andreas Neofytou
anneofytou@ucsd.edu

[1] Structural Engineering Department, University of California San Diego, San Diego, CA 92093, USA

[2] Honda Research Institute Europe, 63073 Offenbach/Main, Germany

[3] NUMETO, 43-190 Mikolow, Poland

Published online: 10 April 2025

measure of noise and is used as a standard measure for noise in many national and international standards and regulations.

The primary objective here is to minimize the acoustic pressure at given locations inside a cabin for different excitation frequencies by optimizing the topology of the vehicle's floor. The floor is selected here since it has been shown to be one of the main panels contributing to the acoustic pressure in the cabin (Chen et al. 2015; Zheng et al. 2015); however, the methodology can be applied to any other parts. We generate optimized 3D designs through a series of experiments, where we vary the frequency and boundary conditions, and compare the designs. We investigate the effects of volume and stress constraints to account for material usage and structural capability. A similarity constraint (Yousaf et al. 2020) is also explored to generate symmetric designs under asymmetric boundary conditions. The proposed method has been developed with generalization in mind, so that it can be extended to larger-scale problems and to different types of vehicles including automobiles and aerospace applications.

The mLSTO method used has several key advantages for multiphysics problems like acoustic-structure interactions. First, the optimization formulation is decoupled from the sensitivity computation algorithm. This is made possible through a discrete adjoint approach which is based on a local boundary perturbation scheme (Kambampati et al. 2020). This approach maps element-based sensitivities to shape sensitivities on the boundary. Any software of choice can be used for solving the governing equations and automatic differentiation (AD) can be used to compute the element sensitivities. Enabling the use of AD is a key aspect in computing sensitivities, especially for complex problems. Moreover, the modularized nature of the proposed architecture offers freedom in the selection of AD methodology and software. Here, the open-source finite element library FEniCS (Alnaes et al. 2015) is used for solving the vibro-acoustic problem in combination with the AD package Dolfin-Adjoint (Mitusch et al. 2019). Dolfin-Adjoint uses semi-symbolic differentiation, which provides automated sensitivities with very high efficiency.

The remainder of this paper is structured as follows: Sect. 2 gives an overview of the relevant literature. Section 3 provides an overview of the mLSTO architecture. Section 4 outlines the governing equations and the optimization problem formulation. The experiments and main outcomes are discussed in Sect. 5 where a series of different frequencies, constraints, and boundary conditions are investigated. Section 6 provides some concluding remarks and discusses the future goals and possible extensions of this work.

2 Related work

In this section, a review of the relevant literature is outlined. Specifically, previous works that considered the design of vehicles for reduced noise in the cabin are discussed. An overview of works that explicitly used TO for noise minimization is also given.

2.1 Sound-absorbing materials and parametric panel optimization

Several studies have explored the design of vehicles for criteria related to acoustics. Some include distribution of sound-absorbing materials. For example, Lee et al. (2013) developed and evaluated porous fibrous materials. Specifically, hollow polyethylene terephthalate (PET) fibers were used to improve the acoustic performance in the interior. Wu et al. (2019) proposed a method for interior noise reduction by controlling the vibration of the body plate using the phononic crystal theory. A 2D phononic crystal structure with a point defect was applied to the car ceiling. The ceiling was divided into several regions, and each region's contribution to the interior noise was first assessed using the finite element method (FEM), to determine where the oscillators should be mounted. From the analysis, the major peak frequencies contributing to the noise were also identified at 205 Hz, 325 Hz, and 395 Hz to determine the bandgap needed to eliminate these frequencies. The point defect was used to exclude the bandgap frequencies that had a negative contribution, meaning that they improved the acoustic performance. Reductions of up to 38 dB were observed.

Parametric optimization to reduce the body vibrations was also considered by numerous works. Jennewein et al. (2004) presented an interactive optimization software tool that solves the system equations in the modal space. When doing design changes during an optimization cycle, only the system matrices are updated, not the modal matrix. This approximation allows iteration steps to run very quickly and makes it possible to optimize material properties, as well as shape and beading patterns. Guo et al. (2011) analyzed the contribution of the body panels vibration to the structure-borne sound pressure level in the interior of a mini-bus structure. Numerical methods such as FEM and the boundary element method (BEM) were combined with experimental testing to perform the analysis. The frequency range below 200 Hz was the main interest in this study. Based on these results, constraint damping treatments on the most contributing panels were adopted to control the vibration. Reductions of up to 7.4 dB were observed in this study. Kim and Kang (2011) used test-based simulation approaches to identify the effect of the local stiffness on

the interior noise. Local stiffness referred to the stiffness of the mounting points through which vibration energies were transferred from the powertrain to the vehicle body. The local stiffness could then be modified to improve the vibration and harshness performance of the vehicle body and reduce noise. The change in local stiffness was achieved by attaching an additional system such as a steel beam. The attachment was made by adhesion or welding, and the beam played the role of a stiffener to the mounting location. A noise transfer function between the mounting points and the driver's ear was estimated for frequency ranges between 0 and 1024 Hz. Based on their findings, the location and attachment method of the additional stiffener can improve acoustic performance. Chen et al. (2015) presented multi-objective optimization of sound package parameters for reducing the interior high-frequency noise of a heavy-duty truck. Gray relational analysis (Deng 1982) was used to determine the optimal combination of parameters such as the thicknesses of the sound packages for the floor, roof, front wall, and rear wall. For the coupled structural-acoustic analysis, the statistical energy analysis was used. The weight of the sound packages was also included in the objective. The results showed that the sound package of the floor has the strongest effect of all the sound package parameters. The maximum noise reduction observed was 3.51 dB for a frequency of 2500 Hz.

Zheng et al. (2015) studied minimization of the acoustic pressure at the right ear of the driver by considering structural optimization. For the structural-acoustic model, the FEM and modal analysis were used, together with the response surface method (RSM) for fast optimization. An excitation frequency of 75 Hz at the left and right engine mounts was considered. Sensitivity analysis was carried out to find the key panels to be used in optimization. Out of 45 panels, only the ten with the highest sensitivity values were selected for optimization and their thicknesses were used as the design variables. The stiffness, the first mode frequency, and weight were used as constraints. A 9 dB reduction of sound pressure level in the right ear of the driver was obtained through geometric optimization of the panels. Further reductions of up to 15 dB were achieved by an additional evolutionary TO to optimally distribute the layout of damping material. TO was only used for the front floor as it was found to be the key panel resulting in the maximum contribution to sound pressure. The work by Lu et al. (2017) presented a method to optimize the peak responses of low-frequency vibrations for improving the NVH performance of a vehicle body. Engine excitation frequencies up to 121 Hz were considered. A response sensitivity analysis was performed to identify the panels with the most significant influence on the interior noise and the thicknesses of those panels were used as design variables. For optimization, the RSM and the adaptive simulated annealing (ASA) metaheuristic algorithm were used. Reductions of up to 3 dB were obtained along with a slight increase in natural frequencies. Zhang et al. (2018) considered the low-noise structural optimization of a heavy commercial vehicle cabin. Specifically, the objective was to reduce the sound pressure level at the right ear of the driver at 169 Hz. The finite element model and structure-acoustic coupled model of the vehicle cabin were developed while the vibration signals at four car suspensions were obtained through a series of vibro-acoustic tests with varying running speeds. A panel acoustic contribution analysis was performed to obtain the panels contributing the most to the acoustic pressure level at the right ear of the driver at the low-frequency range below 200 Hz. These were the roof, back panel, and floor, whose thicknesses were used as the design variables. For optimization, a mathematical surrogate model was constructed by radial basis function (RBF), and the problem was solved using a genetic algorithm. Reductions up to 8.11 dB were achieved.

2.2 Topology optimization for noise reduction

Reducing noise can be achieved indirectly when considering objectives that are not strictly related to sound. The works following this approach did not consider the coupled acoustic-solid problems, rather, they considered only the structural part. The radiated sound was reduced as an indirect consequence of either dynamic compliance minimization (Olhoff and Du 2014; Yang and Li 2013) or maximization of the fundamental and higher frequencies (Du and Olhoff 2006; Picelli et al. 2015; Pedersen 2000).

Considering objectives that are directly related to noise, several works looked at noise reduction by modeling only the acoustic domain and setting the generated noise as a source term. For example, Kim and Yoon (2015) developed an acoustic TO considering porous and rigid materials simultaneously to design noise barriers, with the objective of minimizing the SPL at a receiver point. Duhring et al. (2008) considered acoustic design and density-based TO to reduce the sound level in certain parts of a room by an optimized distribution of reflecting material along the walls. Single frequencies and frequency intervals were considered for both 2D and 3D problems, with noise reductions up to 30 dB. Azevedo et al. (2018) proposed an acoustic muffler design procedure using the bi-directional evolutionary structural optimization (BESO). The objective was to find the best configuration of 2D barriers, represented by rigid wall boundary conditions, to minimize the SPL in the outlet of the muffler. Guo et al. (2020) considered the noise shielding effect that balconies have in high-rise apartments. The objective was to enhance noise mitigation by optimizing the shape of the ceiling of a two-dimensional simplified

urban building. LSTO was employed in this study with shape sensitivity analysis using the continuous adjoint method.

Direct noise minimization, considering acoustic-structural system, deals with noise generated in an acoustic medium through the vibrations of a structure. In this case, the two domains interact through the acoustic-structural interface (ASI). Some works considered an ASI that remained unchanged throughout optimization. Typically the solid was either a 2D or 3D plate interacting with an acoustic medium through the top surface of the plate. TO was used to optimize the material within the plate, without changing the shape of the plate. In this case, there was no need for tracking the ASI throughout optimization which avoided the design dependency of the problem. Some examples include the density-based TO works by Du and Olhoff (2007) and Du and Olhoff (2010). In these works, one-way coupling was also assumed, ignoring the contribution of the acoustic solution on the solid equations. Zhang et al. (2017) used a similar methodology but considered a fully coupled system to minimize the radiated sound power from a vibrating structure within a frequency range. Instead of simple plates, in this case, the 3D structure of a compressor housing was used. The shape of the structure remained unchanged throughout optimization, and the stiffness distribution on the surface was optimized using density-based TO. Several authors considered the fully coupled acoustic-structure interaction systems with evolving ASI. Density-based methods typically handle the need for tracking an ASI through a mixed displacement–pressure formulation as used by Yoon et al. (2007). Instead of two separated domains, in this work, a single domain was employed, and each finite element had both pressure and displacement degrees of freedom, to switch between the linear elastic solid and the acoustic medium governed by the Helmholtz equation. To obtain a stable solution, displacement variables should use higher-order interpolations than the auxiliary pressure variable (Dilgen et al. 2019). Based on this mixed formulation and the Ersatz material model, Hu et al. (2020) proposed a floating projection TO method to minimize the sound pressure at a designated domain for 2D and 3D examples.

LSTO, on the other hand, provides well-defined boundaries and allows for separated solid and acoustic domains. Isakari et al. (2017) considered 3D acoustic-structure interaction for reducing the sound level at some fixed observation points using BEM coupled with a FEM solver. Desai et al. (2018) also considered 3D acoustic-structure interaction to minimize acoustic pressure in a volume target domain under a volume constraint, and investigated the analytical derivation of surface-dependent terms in the shape derivative. Kliewe et al. (2022) optimized the positioning of a bead on a thin plate in order to reduce the noise generated in the fluid region. Dilgen and Aage (2021) used the explicit level-set method in combination with the cut fem method to minimize the radiated acoustic pressure in transient coupled acoustic-mechanical interaction 2D problems. The CutFEM method realizes the exact boundary representation through sub-element integration which is carried out for the elements that are cut by a non-conforming boundary. Dilgen et al. (2022) focused on the application of 3D, large scale, Behind The Ear (BTE) type of hearing instruments, using the same explicit level-set/CutFEM methodology. In this work, the authors modeled fully coupled acoustic-structure interaction in the frequency domain. The aim was to design the internal tube transferring the signal to the ear in order to minimize the acoustic pressure at the microphone surface. Five discrete frequencies in the range of 1kHz–3kHz were considered in the objective, and a volume constraint was not utilized.

2.3 Motivation

In this work, we are using the LSTO to consider noise minimization involving one-way coupled acoustic-structure interaction in a 3D design domain with a fixed ASI. The part of the previous literature that uses parametric optimization mainly focuses on altering a set of parameters of the panels, such as the thickness, through sizing optimization. The overall topology of the existing design, however, remains unchanged. TO, on the other hand, allows for altering the topology, and thus, offers more design freedom and can potentially lead to innovative designs for noise minimization. In this paper, we propose an mLSTO methodology for improving the acoustic performance in the interior of vehicles. To this end, a simplified vehicle cabin shape is used. The consideration of very detailed, large-scale models such as the ones used in the outlined literature poses additional computational challenges for TO, which are beyond the scope of this paper. Nevertheless, the presented methodology can be extended to address these aspects, and this will be the focus of our future efforts. An in-depth discussion of the merits of the mLSTO compared to traditional methods can be found in Jauregui et al. (2023) and Kambampati et al. (2020). For vibro-acoustic problems specifically, a major benefit of the proposed methodology even compared to other level-set methods is its generality. The modular architecture allows for any solid and acoustic solvers to be used according to what the application at hand needs and AD ensures robust differentiation of any objective and constraints of interest. This includes open-source tools as we demonstrated here with FEniCS and also commercial software as explained by Guibert et al. (2024). Another benefit of the method, especially compared with traditional density-based TO, is the explicit level-set

boundary representation, leading to a well-defined ASI. Since density-based TO lacks well-defined boundaries, additional numerical techniques are required (Yoon et al. 2007).

In addition to noise minimization, we incorporate structural performance in the form of stress constraints to ensure the capability of the obtained designs to carry loads. The works by Shu et al. (2014) and Dilgen et al. (2022) discussed the possibility of trivial solutions in which the optimizer either tries to remove all solid material altogether, or disconnects the region of external loads to isolate the acoustic system from the structural excitation. Shu et al. (2014) used a volume constraint to avoid the removal of all solid material, and non-design domains where used to keep the structure fully connected. For the examples studied by Dilgen et al. (2022), non-design domains were also used to not allow for trivial solutions and, thus, a volume, or stress constraints were not used. However, in the automotive applications of interest in this paper, structural performance cannot be neglected, and thus, it is incorporated in the formulation. As evident from the literature, when stress constraints are included in combination with other physics, the results can drastically change. For example, de Leon et al. (2015) and Meng et al. (2021) illustrated the difference in the optimized designs with and without stress constraints for compliant mechanisms and thermal structures, respectively. In addition, the highly nonlinear and non-monotonic behavior of stress constraints as discussed in Le et al. 2010 results in a complex design space. The incorporation of stress constraints in combination with the acoustic pressure minimization is a major novelty in this work compared to the aforementioned TO works.

The remainder of the paper is organized as follows: Sect. 3 gives an overview of the modularized LSTO methodology. Section 4 outlines the governing equations, and Sec. 5 discusses our numerical investigations and optimization results. Sec. 6 provides some concluding remarks.

3 Modularized level-set topology optimization (mLSTO) methodology

In this section, the basic concepts of the mLSTO method are outlined. For a more in-depth discussion, the reader is referred to Jauregui et al. (2023) and Kambampati et al. (2020).

The structure is defined implicitly based on the level-set field as follows:

$$\begin{cases} \phi(\mathbf{x}) \geq 0, & \mathbf{x} \in \Omega, \\ \phi(\mathbf{x}) = 0, & \mathbf{x} \in \Gamma, \\ \phi(\mathbf{x}) < 0, & \mathbf{x} \notin \Omega, \end{cases} \tag{1}$$

where $\phi(\mathbf{x})$ is the level-set function evaluated at point $\mathbf{x}$, Ω is the domain of the structure, and Γ is the structural boundary. The level-set function is updated at each optimization iteration by solving the following level-set advection equation (Osher et al. 2004):

$$\frac{d\phi}{dt} + |\nabla\phi(x)|V_n(x) = 0, \tag{2}$$

which is commonly discretized as follows:

$$\phi_p^{k+1} = \phi_p^k - \Delta t|\nabla\phi_p^k|V_{n,i}, \tag{3}$$

where p is a nodal point on the level-set grid, k is the iteration number, $\nabla\phi$ is the level-set function gradient, computed using the Hamilton–Jacobi weighted essentially non-oscillatory scheme (HJ-WENO), and $V_{n,i}$ is the normal velocity.

The velocity field needed to solve Eq. (2) is obtained by solving the following linearized optimization problem:

$$\begin{aligned} \underset{V_{n,i}}{min} \quad & \Delta F = \sum_i^{n_p} \left(\left(\frac{\partial F}{\partial \Omega} \right)_i A_i z_i \right), \\ s.t. \quad & G_j = \sum_i^{n_p} \left(\left(\frac{\partial G_j}{\partial \Omega} \right)_i A_i z_i \right) \leq g_j^t \quad j = 1, 2, ..., N_g, \\ & -m_i \leq z_i \leq m_i, \end{aligned} \tag{4}$$

where n_p is the number of boundary points, $z_i = V_{n,i}\Delta t$ is the movement of the i^{th} boundary point, the pseudo-time step $\Delta t = 1$, A_i is the area of the discretized boundary associated with the i^{th} boundary point, g_j^t is the target constraint value for the j^{th} constraint, and m_i is the boundary movement limit. The terms $\frac{\partial F}{\partial \Omega}$ and $\frac{\partial G_j}{\partial \Omega}$ represent the boundary shape sensitivities of the objective function and the j^{th} constraint, respectively. Conventionally, these shape sensitivities are computed based on the continuous adjoint method (Allaire et al. 2004; Wang et al. 2003; Dunning and Kim 2015; Picelli et al. 2018).

A unique feature of this mLSTO method is a procedure that allows for the use of the discrete adjoint method or AD in the context of the traditional LSTO (Kambampati et al. 2020). This is achieved through a mapping function that converts element sensitivities into shape sensitivities at the level-set boundary. The architecture is illustrated in Fig. 1.

The overall process can be divided into three separate modules (Fig. 1): The design update module which includes the optimization algorithm for the design update, the state equation solving module in which the governing PDE is

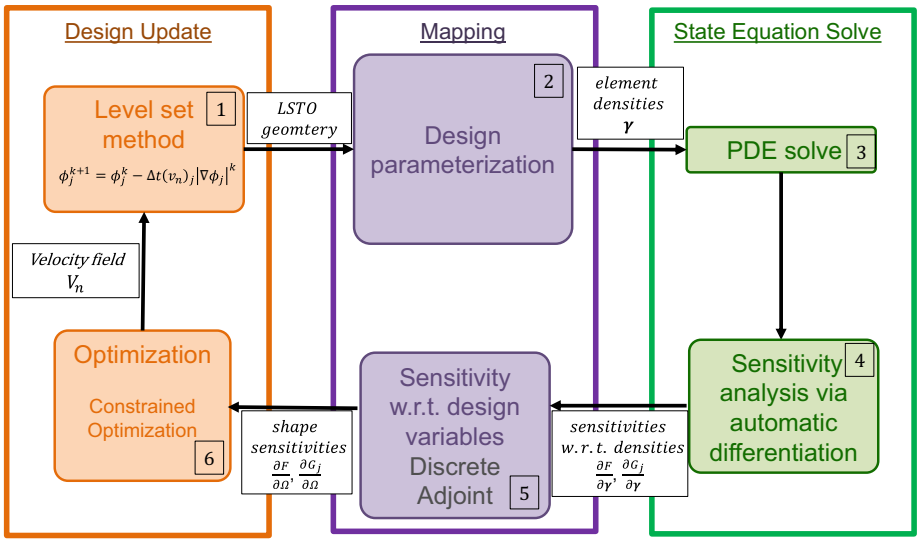


Fig. 1 Modularized LSTO architecture

solved to obtain the sensitivities of the objective F and constraints G with respect to the design variables $\boldsymbol{\gamma}$, and a mapping function that communicates the design information between the two. This mapping is necessary in the case of LSTO, since the level-set field grid does not need to be the same as the analysis mesh. Thus, the design parametrization and sensitivity computation need to be communicated between the two discretized domains. This can be done in a number of ways, for example, by employing conforming meshes (Allaire et al. 2014) or by using immersed methods such as the extended finite element method (XFEM) (Jenkins and Maute 2016) and the finite cell method (FCM) (Cai et al. 2014). In the mLSTO used here, the level-set field (box 1) is mapped onto the analysis mesh using the Ersatz material approximation. A density field, $\boldsymbol{\gamma}$, is created on a regular fixed analysis mesh based on the area fractions of the elements, as these are obtained from the location of the boundary and the level-set field. These area fractions are computed for each element as the area of the element over which $\phi \geq 0$ divided by the total area of the element. Elements that lie entirely inside the structure ($\phi \geq 0$) are structural elements with a density property $\boldsymbol{\gamma} = 1$, elements that are completely outside ($\phi < 0$) are void and have density values $\gamma = \gamma_{\min}$, where $\gamma_{\min}$ is a small some small value to guarantee numerical stability, and elements that are cut by a boundary have intermediate density values $\boldsymbol{\gamma}_{min} \leq \boldsymbol{\gamma} \leq 1$. The density field constructed on the fixed mesh acts as a set of design variables that map the design onto the analysis mesh, which is one functionality of the mapping (box 2). Now, the material properties are interpolated using the density field and the PDE can be solved (box 3), while the element sensitivities can be obtained using the discrete adjoint method, or AD (box 4). Here, any combination of a PDE solver and an AD tool can be used in a plug-and-play fashion. The mapping function is then used again to map these element-based sensitivities onto the boundary as shape sensitivities (box 5) and the optimization problem in Eq. (4) is solved to obtain the boundary point velocities and update the level-set field (box 6).

The original LSM method described in this section along with the optimization component is written in C++ and is freely available.[1] Different options are available for optimization algorithms through external open-source dependencies such as NLopt (da Silva 2022), GLPK (Makhorin 2012) and our in-house Newton–Raphson implementation. The mapping function is also handled by the LSM implementation. In order to implement the modular architecture, these need to be wrapped such that they can link the LSM to the PDE solver of choice. Since FEniCS is a python software, the Cython language (Behnel et al. 2011) was used to wrap the LSM and mapping modules into a shared object file that can be imported in to python to allow communication with FEniCS. This implementation is applicable to any C++ or python solvers and can be accessed through the corresponding repositories.[2,3] Similar wrappers can be developed for communication with commercial packages, as done for example in Jauregui et al. (2023) and Guibert et al. (2024).

4 Problem formulation

The governing equations and the optimization formulation are discussed in this section. Assuming harmonically varying pressure, the acoustic domain is governed by the Helmholtz equation:

[1] http://m2do.ucsd.edu/software/.

[2] https://gitlab.com/m2dO1/paralesto.

[3] https://zenodo.org/record/7613753#.Y-LyCezMK3I.

$$\nabla \cdot \left(\frac{1}{\rho_a} \nabla p \right) + \frac{\omega^2 p}{\rho_a c_a^2} = 0 \quad \text{in} \quad \Omega_{acoustic}, \tag{5}$$

where p is the acoustic pressure, $\nabla \cdot (\nabla p)$ is the Laplacian of pressure, ρ_a is the density of the acoustic medium, ω is the frequency, and c_a is the wave propagation velocity. Different options of acoustic boundary conditions for solving the Helmholtz equation include the following:

- Pressure boundary condition: $p = p_0$,
- Acceleration boundary condition: $\mathbf{n} \cdot \nabla p = \alpha_0$,
- Hard wall condition: $\mathbf{n} \cdot \nabla p = 0$,
- Sommerfeld boundary condition: $\mathbf{n} \cdot \nabla p + i \cdot k \cdot p = 2i \cdot k \cdot p_{in}$,

where p_0 is the imposed pressure, $\mathbf{n}$ is the outward unit vector normal to the acoustic medium, α_0 is the input acceleration, and p_{in} is the pressure amplitude of an incoming wave.

The solid domain is governed by the dynamic equation expressed as follows:

$$\nabla \cdot \sigma + \omega^2 \rho_s \mathbf{u} = 0 \quad \text{in} \quad \Omega_{solid}, \tag{6}$$

where σ is the stress tensor, $\nabla \cdot \sigma$ is the stress gradient, ρ_s is the solid density, and $\mathbf{u}$ is the displacement vector.

The interface condition for the acoustic domain at the ASI is given by

$$\mathbf{n} \cdot \nabla p = \omega^2 \rho_a \mathbf{n}^T \mathbf{u} \quad \text{at} \quad ASI. \tag{7}$$

In this work, the position of the ASI remains fixed, and thus, the acoustic domain is predefined and remains unchanged throughout optimization. Furthermore, the acoustic pressure acting on the structure is neglected, since the resulting displacements are negligible. Consequently, the equations can be solved sequentially by first determining the displacements in the solid domain, which are then imposed on the acoustic domain.

The automotive structural designs are typically analyzed for a discrete set of characteristic excitation frequencies. These frequencies are derived from the behavior of different parts of the vehicle, such as the engine, wheels, and suspension. For this purpose, a weighted objective function is considered. The total objective function J_{tot} is formulated as follows:

$$J_{tot} = \sum_{f=0}^{N_f} w_f J_f(\omega_f), \tag{8}$$

where N_f is the total number of individual frequencies, w_f are the weights, ω_f is the f^{th} frequency, and $J_f(\omega)$ is expressed as follows:

$$J_f(\omega_f) = \mathbf{p}(\omega_f)^T_{\mathbf{x_p}} \cdot \mathbf{p}(\omega_f)_{\mathbf{x_p}}, \tag{9}$$

where $\mathbf{x_p}$ are the coordinates of the nodes at which the acoustic pressure is to be minimized, and $\mathbf{p}$ is the vector containing the acoustic pressure values at points $\mathbf{x_p}$. Minimizing pressure at selected points enables the design to meet specific criteria at designated points, which can be crucial for applications with localized sensitivity, such as reducing noise at a driver's ear in automotive design. It should be pointed out, however, that the optimized design might be overly sensitive to small changes in the environment or usage conditions that affect the selected points differently than the rest of the domain. This could result in a design that performs well at the specified points but not necessarily elsewhere (Marburg 2002). More investigations on different points are discussed in Sec. 5.5.

The optimization problem can then be formulated as follows:

$$\begin{aligned} &\textit{minimize} \quad J_f(\omega_f) = \mathbf{p}(\omega_f)^T_{\mathbf{x_p}} \cdot \mathbf{p}(\omega_f)_{\mathbf{x_p}} \\ &s.t. \quad G_j \leq 0 \quad j = 1, 2, ..., N_g, \\ &\qquad \nabla \cdot \left(\frac{1}{\rho_a} \nabla p \right) + \frac{\omega^2 p}{\rho_a c_a^2} = 0, \quad in \quad \Omega_{acoustic} \\ &\qquad \nabla \cdot \sigma + \omega^2 \rho_s \mathbf{u} = 0, \quad in \quad \Omega_{solid}, \end{aligned} \tag{10}$$

where G_j represents the j^{th} constraint and N_g denotes the total number of constraints. Volume and stress constraints will be considered in the following sections.

5 Numerical investigations

The case studies presented in this section investigate the effects of different frequencies, constraints, and boundary conditions on reducing the acoustic pressure at points of interest inside the 3D acoustic domain.

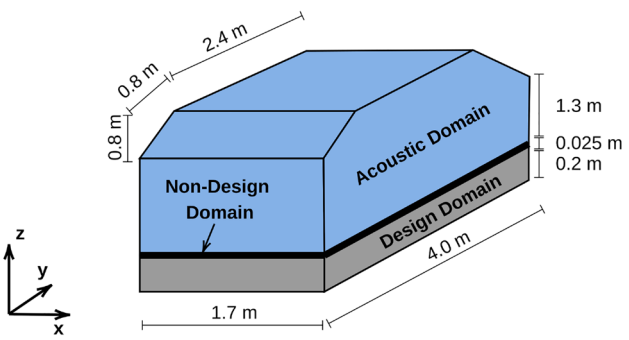


Fig. 2 Boundary conditions applied to the coupled acoustic-structure domain

5.1 Design domain and boundary conditions

The objective is to minimize the acoustic pressure at point **P** in a prototypical vehicle cabin by modifying the topology of the vehicle's floor, which vibrates due to the vertical contact forces (Fig. 2). The TO takes place in a 20-centimeter-thick space in the vehicle floor. The design solid domain is discretized with 8000 linear hexahedral brick elements, each with displacement degrees of freedom (DOF), whereas the acoustic domain is discretized with 13,200 linear hexahedral brick elements, each with a single-pressure DOF. The non-design interface between the floor and the acoustic domain is 2.5 cm. The design domain considered here has Young's modulus $E = 69\ GPa$, Poisson's ratio 0.3, density $\rho = 2730\ kg/m^3$ whereas the acoustic medium is considered to be air with density $\rho_{air} = 1.21\ kg/m^3$. All the walls have hard wall boundary condition: $\mathbf{n} \cdot \nabla p = 0$, where $\mathbf{n}$ is the normal vector and p the acoustic pressure. The design domain is loaded with two vertical harmonic loads $F_1 = F_2 = F_0 e^{-i\omega t}$ of maximum amplitude of F_0 at the two front corners, whereas the corners at the back are fixed in all displacement DOF. These point loads represent mounting points through which vibration energy is typically transferred to the interior of the vehicle. The computational analysis was conducted on a high-performance workstation running Ubuntu 22.04.3 LTS, equipped with an Intel ® Xeon ® Gold 6130 CPU @ 2.10GHz (x86_64 architecture), 384 GB of RAM, and a 2.0 TB storage capacity. The average

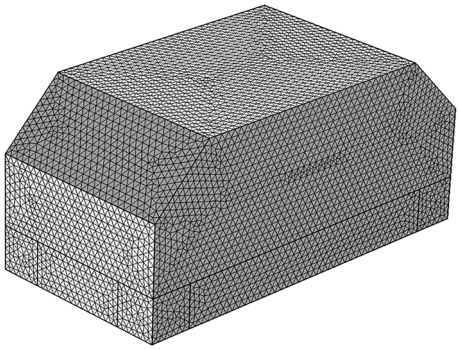
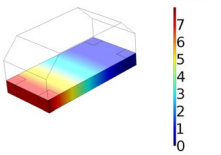
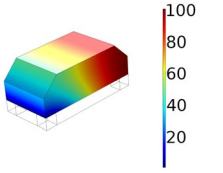
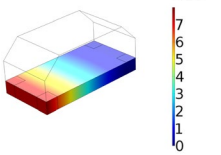
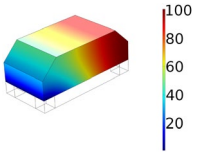
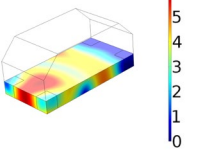
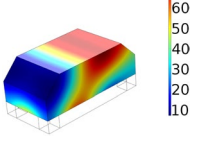
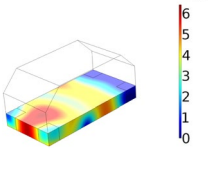
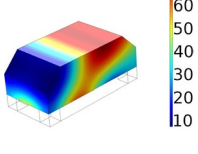
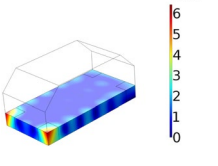
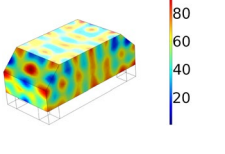
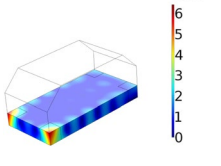
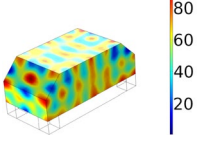


Fig. 3 Conforming mesh for the setup in Fig. 2

Table 1 Displacement and pressure fields comparison between fully coupled and one-way coupled formulation for 1 Hz, 100 Hz, and 500 Hz

	Fully-Coupled		One-Way Coupled	
	Displacement (m)	Pressure (Pa)	Displacement (m)	Pressure (Pa)
1 Hz				
100 Hz				
500 Hz				

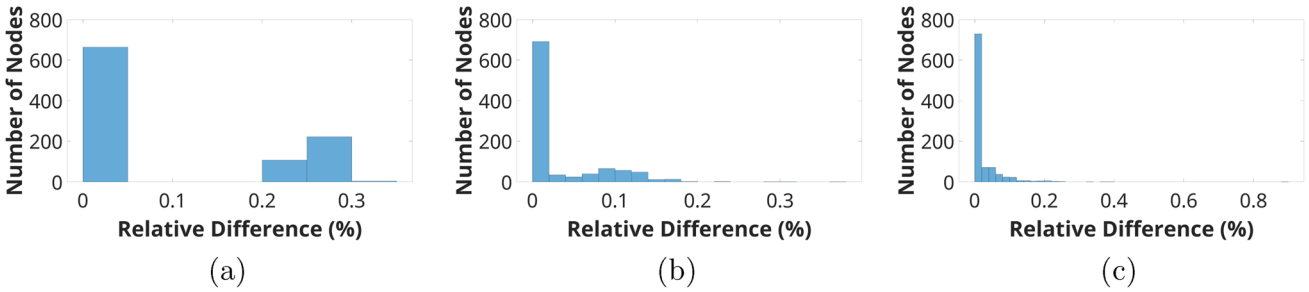


Fig. 4 Error histograms for the solid displacement difference between the fully coupled and the one-way coupled cases for **a** 1 Hz, **b** 100 Hz, and **c** 500 Hz

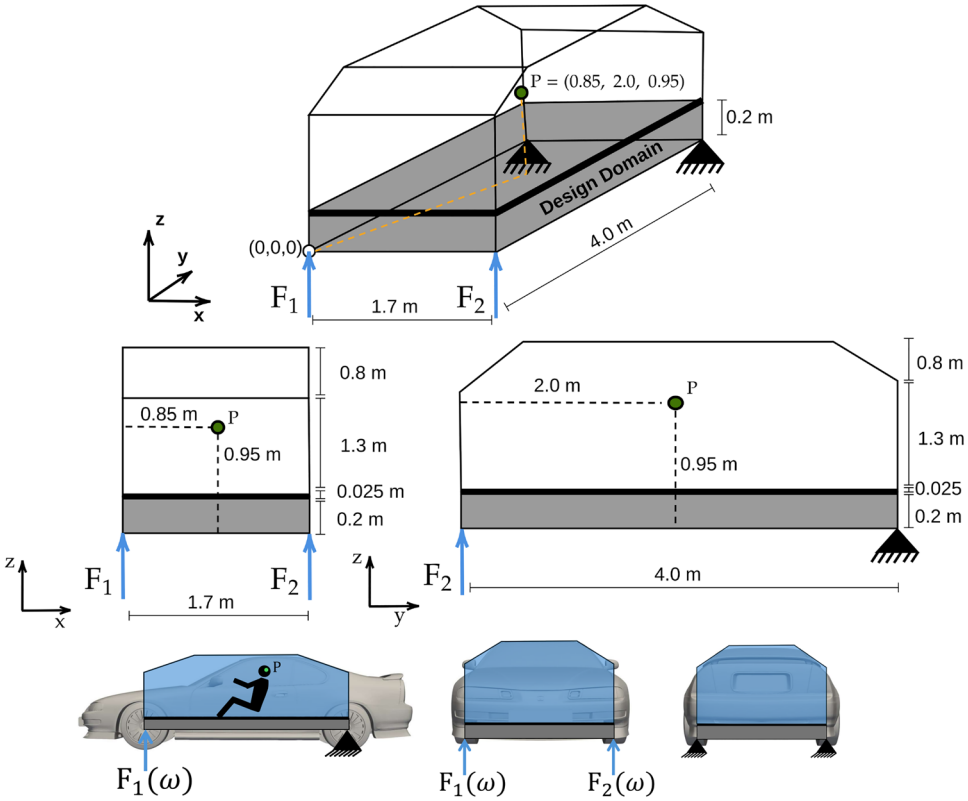


Fig. 5 Problem definition for multiple-frequency investigation. The displacements and rotation at the back corners are fixed in all directions, while the structure is loaded with two vertical harmonic loads at the front corners

time per optimization iteration was 1.5 min per optimization iteration.

5.2 One-way coupling validation

In order to test the assumption that the considered scenario can be treated as a one-way coupled problem, in this section, we compare the displacement and pressure solutions between full coupling and one-way coupling for the setup in Fig. 2. A conforming mesh analysis was employed for this study (Fig. 3). Table 1 shows the results for three different frequencies, 1 Hz, 100 Hz, and 500 Hz. Since we are ignoring the effect of the acoustic pressure solution on the solid governing equations, the histograms in Fig. 4 show the difference in the norm of displacement at each node between the fully coupled and the one-way coupled cases.

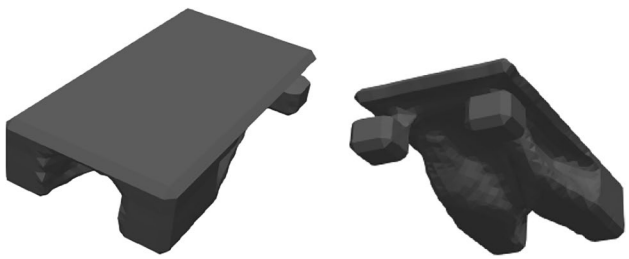
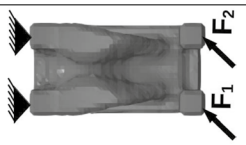
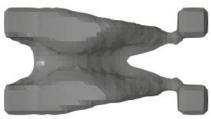
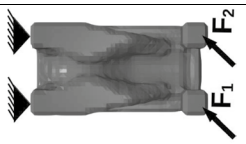
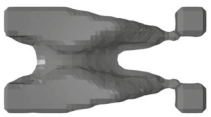
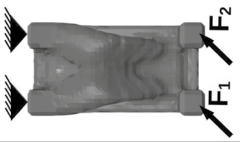
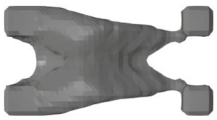
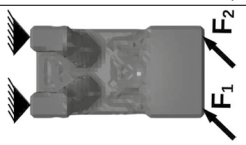
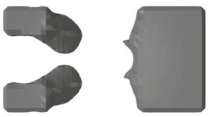
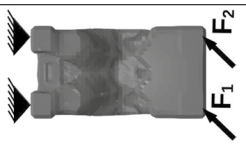
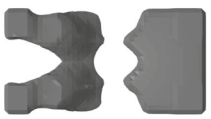
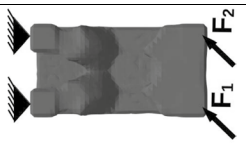
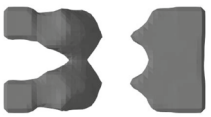
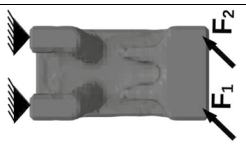
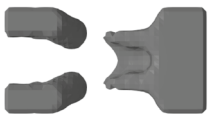
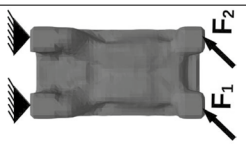
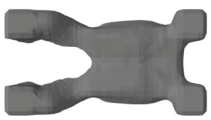


Fig. 6 Optimized design for acoustic pressure minimization using the setup shown in Fig. 5, with a frequency of 1 Hz

Table 2 Optimized solutions obtained for all the different excitation frequencies individually

Frequency	Optimized Solution, Bottom View	Optimized Solution, Bottom View with Interface Removed	Optimized Solution, Side View	Objective, Initial (dB)	Objective, Final (dB)
1 Hz				82.60	84.65
100 Hz				85.28	88.94
200 Hz				95.58	97.62
300 Hz				86.01	25.07
400 Hz				95.95	56.56
500 Hz				90.05	67.67
600 Hz				96.68	92.09
1000 Hz				86.98	62.31

As can be seen in Fig. 4, the relative difference in the displacements is less than 1%, indicating that considering one-way coupling for this specific problem is a viable assumption.

5.3 Optimization for multiple frequencies

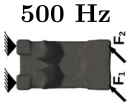
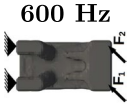
A range of different frequencies is investigated here between 1 and 1000 Hz for the design domain shown in Fig. 5. The design domain is loaded with two vertical harmonic loads $F_1 = F_2 = 1000e^{-i\omega t}$ of maximum amplitude of 1000 N at the two front corners, whereas the corners at the back have the displacement and rotations fixed in all directions. The acoustic pressure at point $\mathbf{P} = \{0.85\ m, 2\ m, 0.95\ m\}$ is to be minimized. Since weight is an important factor, a volume constraint of 60 % is used.

The optimized designs for each individual frequency are shown in Table 2. An example of a full 3D design is shown

in Fig. 6 for the 1 Hz case, with the non-design interface. However, to better show the topologies, the bottom views are provided in the second column of Table 2. To present the details of each design, the top interface is removed in the third column, and the fourth column shows the side view. The two last columns in the table provide the initial and final objective values in decibels (dB).

The first observation is that all the optimized designs are symmetric, and different frequencies lead to different topological features. For example, for frequencies below 300 Hz, thin supports appear near the loading points whereas the supports become much thicker near the pinned corners. The opposite happens for frequencies in the range of 300–1000 Hz where the support is very thick near the loading points and becomes thinner near the pinned corners. Looking at the objective values, for frequencies below 300 Hz, the optimized designs achieve objective values about the same as the initial values, even when 40 % of the material

Table 3 Crosschecking of the optimized designs by testing their performance in the other frequencies. The final objectives normalized by the initial objective value appear in the table

Optimized Designs	Crosschecking Frequencies							
	1 Hz	100 Hz	200 Hz	300 Hz	400 Hz	500 Hz	600 Hz	1000 Hz
1 Hz 	**1.03**	7.80	6.13	2.65	3.45	78.43	22.51	42.45
100 Hz 	3.40	**1.04**	7.24	68.52	162.50	48.14	260.42	87.02
200 Hz 	1.39	1.06	**1.02**	10.76	15.72	4.71	12.52	8.01
300 Hz 	35.44	41.89	1.06	**0.29**	0.32	0.42	0.45	2.38
400 Hz 	524.56	171.68	47.20	8.58	**0.59**	53.64	10.19	23.60
500 Hz 	283.86	371.57	433.78	81.08	34.46	**0.75**	245.27	1461.49
600 Hz 	17.81	76.02	2.53	0.53	1.03	1.05	**0.95**	3.74
1000 Hz 	66.24	120.48	199.32	106.32	31.56	72.72	12.00	**0.72**

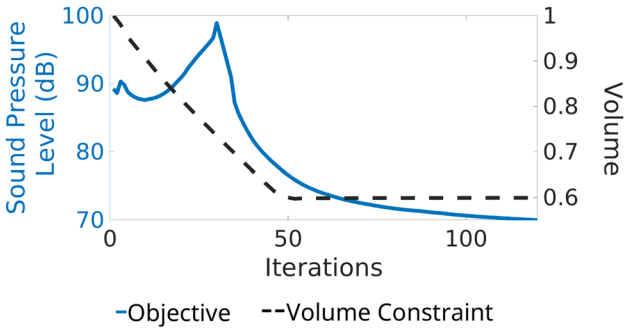


Fig. 7 Objective and volume optimization history for the excitation frequency of 500 Hz

is removed. For frequencies beyond 300 Hz, the objective actually improves even further. The most significant improvement is achieved for the 300 Hz case where a 61 dB reduction is obtained. Significant reductions are also obtained for 400, 500 and 1000 Hz. An example of the sound pressure and volume constraint history is given in Fig. 7 for the 500 Hz excitation frequency.

Crosschecking these results is summarized in Table 3 by testing the optimized design's performances under the rest of the frequencies. Specifically, the optimized design for each frequency is analyzed using as input each of the other frequencies. The normalized objective $\left(\frac{Final\ \ Objective}{Initial\ \ Objective}\right)$, in dB, for each case is provided along the corresponding row in the table. The objective value for the frequency for which each design was optimized is highlighted in blue along the diagonal of the table. As can be seen, the highlighted value is the lowest value in each row. This means that each design performs best when the structure is subjected to the excitation frequency for which the design was optimized.

In Table 4, the optimized results are shown considering three different frequencies in the weighted objective of Eq. (8). Specifically, 100, 500, and 1000 Hz are used simultaneously. Three cases with different weights are tested. In the first case, equal weights are assigned to the three frequencies. Next, a higher weight of 0.8 is given to the 500 Hz frequency while 0.1 is assigned to each of the other frequencies. Lastly, a case with the 1000 Hz frequency having the highest weight of 0.8 is tested. As can be seen by analyzing the results in the table, there are no big topological differences among the obtained designs. In all cases, the final objective value slightly increased compared to the initial value. Table 5 provides the crosschecks for these results against their component frequencies. The designs obtained with the weighted objective are subjected to each of the three frequencies individually. The normalized objectives are shown in rows (d)-(f). For comparison, rows (a)-(c) show again the objective values of the designs obtained for each individual frequency, as given in Table 2. As can be seen, the values in rows (a)-(c) are lower than any value in the rows (d)-(f). If, for example, the goal is to minimize the acoustic pressure at 100 Hz, this design performs better (objective = 0.52) when subjected to 100 Hz than the designs optimized for any of the weighted objectives (objectives = 1.07, 0.84 and 0.79). Moreover, when the high weight is assigned to a frequency, the optimized design performs best when it is subjected to that frequency. For example, when 0.8 weight is assigned to 500 Hz, the objective is lower at 500 Hz (0.84) compared to 100 Hz (0.95) and 1000 Hz (2.39). Similarly, when 0.8 weight is assigned to 1000 Hz, the objective is lower at 1000 Hz (0.16) compared to 100 Hz (0.79) and 500 Hz (0.95).

Table 4 Optimized solutions obtained for a weighted objective function (Eq. (8))

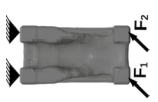
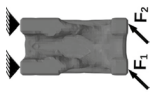
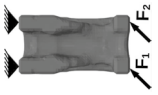
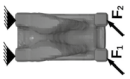
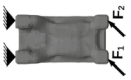
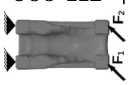
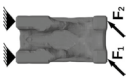
Frequency	Optimized Solution, Bottom View	Optimized Solution, Bottom View with Interface Removed	Optimized Solution, Side View	Objective, Initial (dB)	Objective, Final (dB)
100 Hz + 500 Hz + 1000 Hz				73.52	81.23
0.1·100 Hz + 0.8·500 Hz + 0.1·1000 Hz				73.52	76.11
0.1·100 Hz + 0.1·500 Hz + 0.8·1000 Hz				73.52	75.03

Table 5 Crosschecking of the optimized designs obtained for the weighted objective (8). Testing their performance against their constituent frequencies. The final objectives normalized by the initial objective value appear in the table

Optimized Designs	Crosschecking Frequencies		
	100 Hz	500 Hz	1000 Hz
(a) **100 Hz** 	0.52	-	-
(b) **500 Hz** 	-	0.0037	-
(c) **1000 Hz** 	-	-	0.058
(d) **100 Hz + 500 Hz + 1000 Hz** 	1.07	1.018	1.41
(e) **0.1·100 Hz + 0.8·500 Hz + 0.1·1000 Hz** 	0.95	0.84	2.39
(f) **0.1·100 Hz + 0.1·500 Hz + 0.8·1000 Hz** 	0.79	0.95	0.16

5.4 Optimization within a frequency band

As explained in Sec. 4, the main interest in this work is to reduce acoustic pressure at discrete frequencies that result from vibrations of typical operating conditions. However, to illustrate the generality of our method, we also include a case in which acoustic pressure is minimized within a frequency band. In this example, we first compute a frequency response function (FRF) at point P and up to 1000 Hz, as shown by the blue continuous line in Fig. 8 (b). Two resonance peaks are observed at frequencies around 288 Hz and 676 Hz. We then set the objective to be

$$J_{tot} = \int_{Band\ 1} J_f(\omega_f)d\omega + \int_{Band\ 2} J_f(\omega_f)d\omega, \tag{11}$$

where *Band* 1 and *Band* 2 are the frequency ranges around the 288 Hz and 676 Hz peaks, respectively. Implementation-wise, it should be pointed out that this formulation leads to a nested loop since at each optimization it is required to integrate over multiple-frequency steps within each band to compute the objective and sensitivities. Thus, although the band range can be chosen to be arbitrarily large, the computational cost is a concern. Here, a range of 60 Hz is chosen for each band with a frequency step of 5 Hz. One can vary the band range and step size.

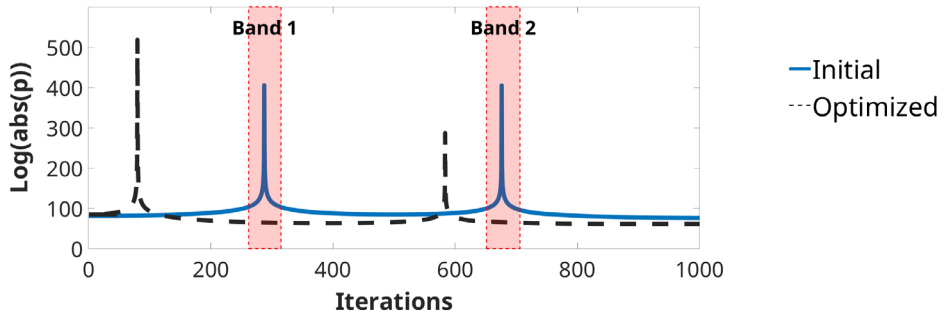
The optimized design is shown in Fig. 8 (a). The corresponding FRF is shown in Fig. 8 (b) by the dashed line. It can be observed that in the optimized design both peaks in acoustic pressure have shifted outside the frequency bands of interest. Moreover, the acoustic pressure is lower in the entire band ranges compared to the initial design.

5.5 Optimization with stress constraint

So far, the optimizations did not take into consideration load-carrying capability. In some cases, designs may lead to high-stress concentrations. For example, the design

Frequencies	Optimized Solution, Bottom View	Optimized Solution, Bottom View with Interface Removed	Optimized Solution, Side View
Band 1: 260-320 Hz + Band 2: 650-710 Hz			

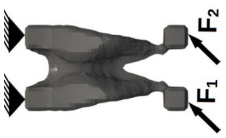
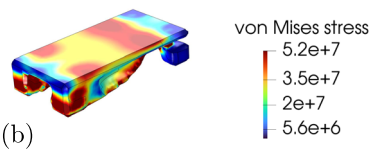
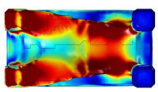
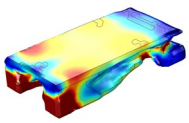
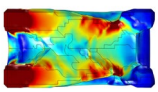
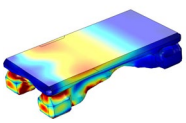
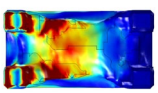
(a)



(b)

Fig. 8 Frequency band optimization

Table 6 Optimized solutions for an excitation frequency of 1 Hz with different stress constraints

Stress Constraint	Optimized Solution, Bottom View with Interface removed	Optimized Solution, von Mises stress 3D View	Optimized Solution, von Mises stress Bottom View
No stress constraint $\frac{\sigma_{max}}{\sigma_{max_0}} = 28$	(a) 	(b) 	(c) 
$\frac{\sigma_{max}}{\sigma_{max_0}} = 20$	(d) 	(e) 	(f) 
$\frac{\sigma}{\sigma_0} = 10$	(g) 	(h) 	(i) 

obtained for an excitation frequency of 100 Hz leads to the von Mises stress distribution shown in Table 6. To reduce high stresses and enhance the capability of the structures to carry mechanical loads while minimizing the acoustic pressure, a stress constraint is added in this section. Here, we use again the design domain shown in Fig. 5, considering the 100 Hz case and assuming a fixed volume constraint of 60%. The p-norm function is used to approximate the maximum stress in the structure:

$$\sigma_{PN} = \left(\int_{\Omega} \sigma_{vm}^{p} d\Omega \right)^{\frac{1}{p}}, \tag{12}$$

where p is the p-norm parameter, σ_{PN} denotes the p-norm stress, and σ_{vm} is the von Mises stress.

In the absence of a stress constraint, the maximum stress σ_{max} in the optimized design is about 28 times higher than that of the initial design, $\sigma_{max,0} = 69.89$ MPa for this example. First, a more relaxed volume constraint is used, requiring σ_{max} to be 20 times higher than $\sigma_{max,0}$. As can be seen in Table 6, Fig. (d), the design in this case has more material gathered near the high-stress region. As a result, stresses are reduced as shown in Figures (e) and (f). The sound pressure level in this case is 96.39 dB which is higher than that without the stress constraint, 88.94 dB. The stresses significantly reduce when σ_{max} is set to be 10 times higher than $\sigma_{max,0}$ as shown in Figures (h) and (i). The additional stress restriction further increases the acoustic pressure to 110 dB. The normalized objective and stress constraint histories are shown in Fig. 9. From the results obtained in this section, it seems that the stress constraint is antagonizing acoustic pressure minimization in this example, with improved stress capability leading to worse noise performance.

5.6 Multiple points of interest and asymmetric boundary conditions

In this section, initial setups that lead to asymmetric designs are investigated, as such conditions can arise in practice when loads and boundary conditions in vehicles are asymmetrical. However, the vehicle itself is largely symmetrical in construction and so symmetry is enforced here to obtain symmetric designs even though the boundary conditions are asymmetric. This symmetry is enforced by defining a symmetry plane as shown in Fig. 12. Then, corresponding elements on the two sides of the symmetry plane can be identified such as elements i and j. The element sensitivities for these two elements are then averaged. For the investigations, a single excitation frequency of 100 Hz is used and a volume constraint of 60 %.

First, a case with two points at which acoustic pressure is to be minimized is studied. The two points are located at the front right corner of the acoustic domain $\mathbf{P_1} = \{1.425\ m, 0.4\ m, 1.75\ m\}$ and at the left back corner $\mathbf{P_2} = \{0.4\ m, 3.0\ m, 1.25\ m\}$, as shown in Fig. 11. The obtained result is asymmetric in this case as shown in column (a) of Table 7. The initial and final acoustic pressure values, respectively, are 93.77 dB and 94.36 dB for $\mathbf{P_1}$ and 85.18 dB and 84.69 dB for $\mathbf{P_2}$. Enforcing symmetry leads to the design in column (b). The final acoustic pressure values for the symmetric design are 94.17 dB for $\mathbf{P_1}$ and 84.89 dB for $\mathbf{P_2}$. The FRF computed at the two points is provided in Fig. 10 for the initial and optimized designs, both symmetric and asymmetric. The FRF behavior is similar at the two points, with peaks around 300 Hz for the initial design. Although the objective is to minimize acoustic pressure at 100 Hz, both the symmetric and asymmetric designs push the peak beyond 300 Hz.

Next, the setup with asymmetric boundary conditions shown in Fig. 11 (b) is considered. The point of interest is the same as in Sec. 5.2, $\mathbf{P} = \{0.85\ m, 2.0\ m, 0.95\ m\}$. The displacement at the front left corner is fixed in all directions. The front right corner is loaded with a vertical harmonic load $F = 1000e^{-i\omega t}$. The displacement at the back right corner is restricted in the z-direction, while the displacement at the back left corner is restricted in the y-direction. The optimized designs for the asymmetric and symmetric cases are shown in columns (c) and (d) of Table 7, respectively. The initial objective value is 90.57 dB. The asymmetric optimized design achieves the final objective of 69.71 dB while the symmetric design results in a higher value of 82.12 dB. This increase in the final

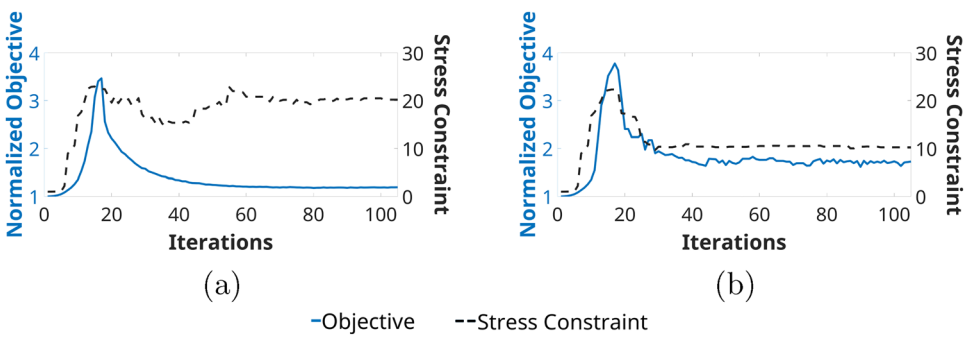


Fig. 9 Normalized objective (objective divided by initial objective) and stress constraint histories for: **a** $\frac{\sigma_{max}}{\sigma_{max_0}} = 20$ and (b) $\frac{\sigma_{max}}{\sigma_{max_0}} = 10$

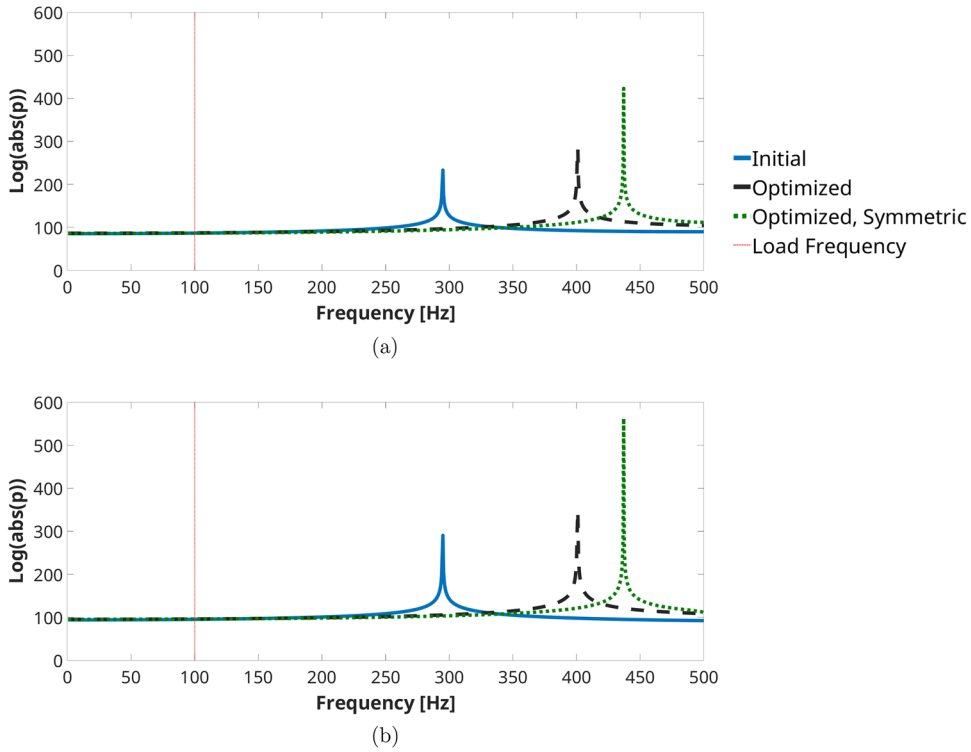


Fig. 10 FRF computed at the two points of interest: **a** $\mathbf{P_1} = \{1.425\ m, 0.4\ m, 1.75\ m\}$ and (b) $\mathbf{P_2} = \{0.4\ m, 3.0\ m, 1.25\ m\}$

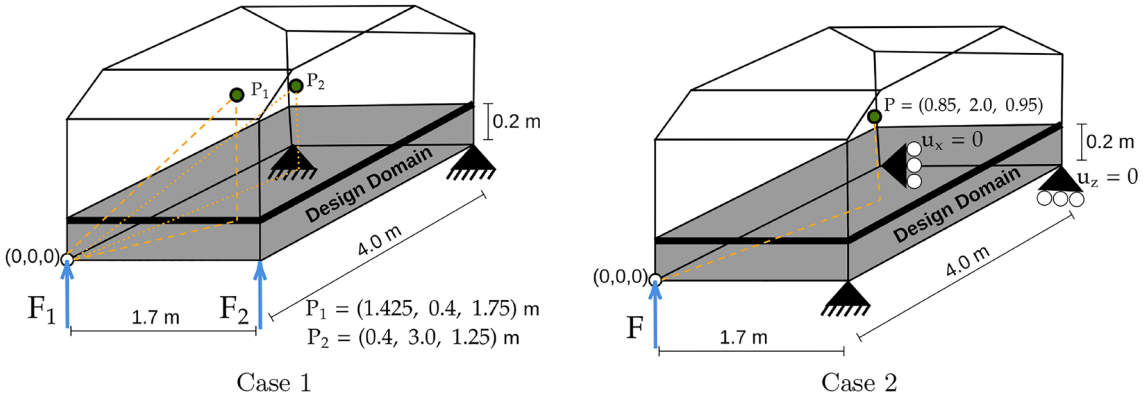


Fig. 11 Two test cases with asymmetric conditions. Case 1: Two points of interest for acoustic pressure minimization and Case 2: Asymmetric boundary conditions

objective can possible be attributed to the requirement of symmetry, which imposes additional restrictions.

Figure 13 illustrates the difference between minimizing acoustic pressure at specific points versus minimizing the average pressure over the volume of the acoustic domain. In Fig. 13 a the optimized design for minimizing acoustic pressure over the volume of the domain is provided. The history of acoustic pressure measured at the two points $\mathbf{P_1}$ and $\mathbf{P_2}$ is given by the solid blue line in Fig. 13b and c, respectively. For comparison, the history of the acoustic pressure measured at $\mathbf{P_1}$ and $\mathbf{P_2}$ for case 1 in Table 7 is given by the dashed black line in Fig. 13b and c, respectively. In case 1, the objective was to minimize acoustic pressure at those specific points, and it can be seen that acoustic pressure for both points is lower when we minimize over the volume. This indicates that simply minimizing the average acoustic pressure may not yield the optimum results if specific points are of interest.

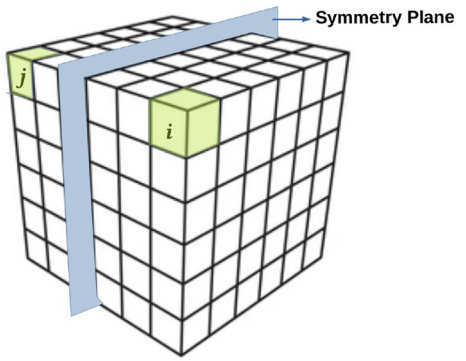
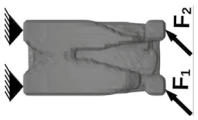
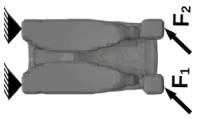
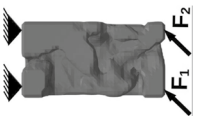
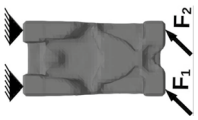
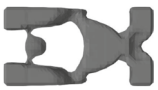


Fig. 12 Symmetry plane with an example of two mirroring elements, i and j

6 Conclusion

In this paper, a modularized level-set topology optimization methodology (mLSTO) was proposed to minimize the acoustic pressure in a 3D domain representing a simplified vehicle cabin. Specifically, noise induced by structural vibrations of the body were the main interest. In addition, we incorporated structural performance in the form of stress constraints. The modularized architecture enables the use of automatic differentiation (AD) in the context of the classical level-set topology optimization to provide automated sensitivities for multiphysics problems such as the acoustic-structure interaction considered here. We evaluated

Table 7 Optimized designs for asymmetric conditions

Optimized Designs	Case 1 (a)	Case 1 with Symmetry (b)	Case 2 (c)	Case 2 with Symmetry (d)
Bottom View				
Bottom View, Interface Removed				
Side View				

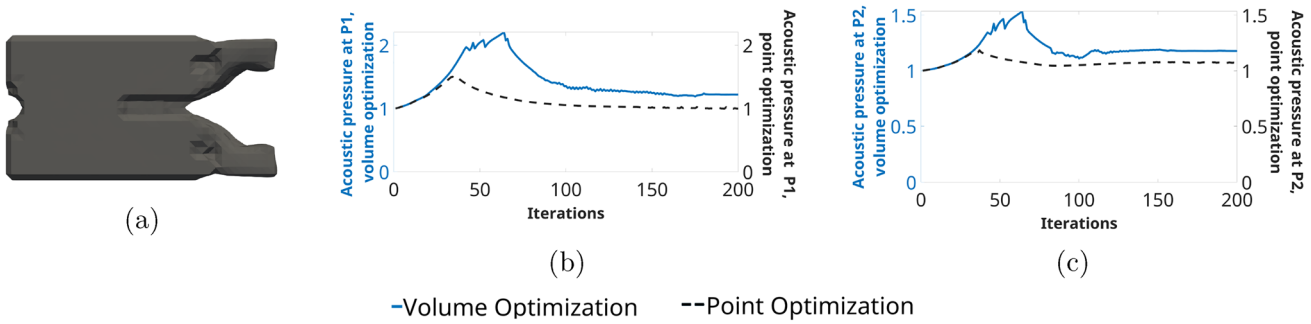


Fig. 13 Minimizing acoustic pressure at a single point versus minimizing the average acoustic pressure over the entire volume of the acoustic domain: **a** Optimized design for minimizing average acoustic pressure over the volume. **b** and **c** Acoustic pressure history at points $\mathbf{P_1}$ and $\mathbf{P_2}$, respectively: solid blue line is obtained through minimization of average acoustic pressure over the volume, dashed black line is obtained through minimization of acoustic pressure at $\mathbf{P_1}$ and $\mathbf{P_2}$

our methodology in a series of 3D topology optimization problems, where we varied the loading conditions and constraints. Designs were obtained for different frequency ranges and stress constraints. In the first set of experiments, we varied the excitation frequency and observed that the designs can change depending on the frequency. In the second set of experiments, we optimized the design for multiple-frequency-weighted objectives. From these cases, we observed that each optimized design performs best when subjected to the excitation frequency for which it was optimized. In the third set of experiments, we optimized the structure for different stress constraint values. In this case, the obtained designs had lower stresses but higher acoustic pressure values. Finally, we tested cases with asymmetric conditions and studied optimized designs with and without enforcing symmetry in the designs. The current work can be extended to more realistic, large-scale problems. Going into larger scales is expected to provide improved solutions with more detailed features which we will address in the next steps of this research. In particular, the reduction of cabin noise in automobiles and (electric) vertical take-off and landing (VTOL) aircraft are potential applications. The proposed methodology can be applied either to optimize the entire body of a vehicle or re-design parts of existing models for improved acoustic performance. These topics will be included in our future investigations.

Supplementary Information The online version contains supplementary material available at https://doi.org/10.1007/s00158-025-03995-z.

Acknowledgements Andreas Neofytou and H. Alicia Kim gratefully acknowledge the financial support from Honda Research Institute Europe (HRI-EU).

Author contributions A.N. wrote the manuscript paper. All authors provided their inputs and expertise throughout the process and reviewed the final manuscript.

Funding Financial support was provided from Honda Research Institute Europe (HRI-EU).

Data availability The optimization was implemented using ParaLeSTO (Jauregui et al. 2023) which is a modular open-source level-set topology optimization code, available at https://doi.org/10.5281/zenodo.7613753. The acousto-structural problem was solved with the open-source finite element software FEniCS (Alnaes et al. 2015) found at https://fenicsproject.org/ and the automatic differentiation was performed with the open-source library Dolfin-Adjoint (Mitusch et al. 2019) available at https://www.dolfin-adjoint.org/en/latest/. The results presented in this paper can be reproduced using the aforementioned open-source software and the methodology described in the paper.

Declarations

Conflict of interest The authors declare that they have no Conflict of interest as defined by Springer, or other interests that might be perceived to influence the results and/or discussion reported in this paper.

Replication of results The optimization was implemented using ParaLeSTO (Jauregui et al., 2023) which is a modular open-source level-set topology optimization code, available at https://doi.org/10.5281/zenodo.7613753. The acousto-structural problem was solved with the open-source finite element software FEniCS (Alnaes et al., 2015) found at https://fenicsproject.org/ and the automatic differentiation was performed with the open-source library Dolfin-Adjoint (Mitusch et al. 2019) available at https://www.dolfin-adjoint.org/en/latest/. The results presented in this paper can be reproduced using the aforementioned open-source software and the methodology described in the paper.

References

Allaire G, Dapogny C, Frey P (2014) Shape optimization with a level set based mesh evolution method. Comput Method Appl Mech Eng 282:22–53

Allaire G, Jouve F, Toader AM (2004) Structural optimization using sensitivity analysis and a level-set method. J Comput Phys 194:363–393

Alnaes MS, Blechta J, Hake J, Johansson A, Kehlet B, Logg A, Richardson C, Ring J, Rognes ME, Wells GN (2015). The fenics project version 1.5. Archive of Numerical Software 3

Azevedo FM, Moura MS, Vicente WM, Picelli R, Pavanello R (2018) Topology optimization of reactive acoustic mufflers using a bi-directional evolutionary optimization method. Struct Multidisc Optim 58:2239–2252

Behnel S, Bradshaw R, Citro C, Dalcin L, Seljebotn DS, Smith K (2011) Cython: the best of both worlds. Comput Sci Eng 13:31–39. https://doi.org/10.1109/MCSE.2010.118

Cai S, Zhang W, Zhu J, Gao T (2014) Stress constrained shape and topology optimization with fixed mesh: a b-spline finite cell method combined with level set function. Comput Method Appl Mech Eng 278:361–387

Chen S, Chen G, Wang D, Song J (2015) Multi-objective optimization of sound package parameters for interior high frequency noise of heavy-duty truck using grey theory. Int J Automot Technol 16:947–957

Deng JL (1982) Control problems of grey systems. System Control Lett 1:288–294

Desai J, Faure A, Michailidis G, Parry G, Estevez R (2018) Topology optimization in acoustics and elasto-acoustics via a level-set method. J Sound Vib 420:73–103

Dilgen CB, Aage N (2021) Generalized shape optimization of transient vibroacoustic problems using cut elements. Int J Num Method Eng 122:1578–1601

Dilgen CB, Dilgen SB, Aage N, Jensen JS (2019) Topology optimization of acoustic mechanical interaction problems:a comparative review. Struct Multidisc Optim 60:779–801

Dilgen SB, Aage N, Jensen JS (2022) Three dimensional vibroacoustic topology optimization of hearing instruments using cut elements. J Sound Vib 532:116984

Du J, Olhoff N (2006) Topological design of freely vibrating continuum structures for maximum values of simple and multiple eigenfrequencies and frequency gaps. Struct Multidisc Optim 34:91–110

Du J, Olhoff N (2007) Minimization of sound radiation from vibrating bi-material structures using topology optimization. Struct Multidisc Optim 33:305–321

Du J, Olhoff N (2010) Topological design of vibrating structures with respect to optimum sound pressure characteristics in a surrounding acoustic medium. Struct Multidisc Optim 42:43–54

Duhring M, Jensen J, Sigmund O (2008) Acoustic design by topology optimization. J Sound Vib 317:557–575
Dunning PD, Kim HA (2015). Introducing the sequential linear programming level-set method for topology optimization. Struct Multidisc Optim 51
Guibert ATR, Hyun J, Neofytou A, Kim HA (2024) Facilitating multidisciplinary collaboration through a versatile level-set topology optimization framework via comsol multiphysics. Struct Multidisc Optim 67:2024. https://doi.org/10.1007/s00158-024-03503-7.
Guo J, Hue Y, Wang MY (2020) Level-set based topology optimization on acoustic balcony ceiling design of a simplified urban building for noise reduction. J Acoust Soc Am 148:3980
Guo R, Zhang LJ, Zhao J, Zhou H (2011) Interior structure-borne noise reduction by controlling the automotive body panel vibration. J Automob Eng 226:943–956
Hu J, Yao S, Huang X (2020) Topology optimization of dynamic acoustic–mechanical structures using the ersatz material model. Comput Method Appl Mechan Eng 372:113387
Isakari H, Kondo T, Takahashi T, Matsumoto T (2017) A level-set-based topology optimisation for acoustic–elastic coupled problems with a fast bem–fem solver. Comput Method Appl Mech Eng 315:501–502
Jauregui CM, Hyun J, Neofytou A, Gray JS, Kim HA (2023). Avoiding reinventing the wheel: reusable open-source topology optimization software. Struct Multidisc Optim 66
Jenkins N, Maute K (2016) An immersed boundary approach for shape and topology optimization of stationary fluid-structure interaction problems. Struct Multidisc Optim 54:1191–1208
Jennewein D, Bohle K, Dunne L, Eng C (2004). Vibro-acoustic parameter optimization of vehicle structures. VDI Berichte , 567–582
Johnson W, Silva C (2018) 2018. Observations from exploration of vtol urban air mobility designs, Asian/Australian Rotorcraft Forum (ARF
Kambampati S, Chung H, Kim HA (2020) A discrete adjoint based level set topology optimization method for stress constraints. Comput Method Appl Mech Eng 377:113563
Kim KH, Yoon GH (2015) Optimal rigid and porous material distributions for noise barrier by acoustic topology optimization. J Sound Vib 339:123–142
Kim KS, Kang YJ (2011) Local stiffness control for reducing vehicle interior noise by using frf-based synthesis method. J Mech Sci Technol 25:81–88
Kliewe P, Laurain A, Schmidt K (2022) Shape optimization in acoustic–structure interaction. Eng Comput 39:172–200
Le C, Norato J, Bruns T, Ha C, Tortorelli D (2010) ess-based topology optimization for continua. Struct Multidisc Optim 41:605–620
Lee J, Lee WLS, Park S (2013). A study for improving the acoustic performance of dash isolation pad using hollow fiber. SAE Tech Paper 2013-01-0101
de Leon M, Daniel Alexandersen, J., Jun, S.J., Sigmund, O., (2015) Stress-constrained topology optimization for compliant mechanism design. Struct Multidisc Optim 52:929–943
Lu J, Zhan Z, Song H, Liu X, Yang X, Yang J (2017). Design optimization of vehicle body nvh performance based on dynamic response analysis. SAE Tech Paper 2017-01-0440
Makhorin A (2012). Glpk (gnu linear programming kit). http://www.gnu.org/software/glpk/glpk.html
Marburg S (2002) Developments in structural-acoustic optimization for passive noise control. Arch Comput Method Eng 9:291–370
Meng Q, Xu B, Huang C, Wang G (2021) Lightweight topology optimization of thermal structures under compliance, stress and temperature constraints. J Thermal Stress 44:1121–1149
Mitusch SK, Funke SW, Dokken JS (2019). dolfin-adjoint 2018.1: automated adjoints for fenicsand firedrake. J Open Source Software 4, 1292
Olhoff N, Du J (2014). Topological design of continuum structures subjected to forced vibration. Topol Optim Struct Contin Mech pp 325–339
Osher S, Fedkiw R, Piechor K (2004) Level set methods and dynamic implicit surfaces. Appl Mech Rev 57:B15
Pedersen N (2000) Maximization of eigenvalues using topology optimization. Struct Multidisc Optim 1:11
Picelli R, Townsend S, Brampton C, Norato J, Kim H (2018) Stress-based shape and topology optimization with the level set method. Comput Method Appl Mech Eng 329:1–23
Picelli R, Vicente W, Pavanello R, Xie YM (2015) Evolutionary topology optimization for natural frequency maximization problems considering acoustic–structure interaction. Finite Elements in Anal Design 106:56–64
Shu L, Wang MY, Ma Z (2014) Level set based topology optimization of vibrating structures for coupled acoustic–structural dynamics. Comput Struct 132:34–42
da Silva Santos C (2022). The nlopt nonlinear-optimization package. http://github.com/stevengj/nlopt
Wang MY, Wang X, Guo D (2003) A level set method for structural topology optimization. Comput Method Appl Mech Eng 192:227–246
Wu X, Zhang M, Zuo S, Huang H, Wu H (2019) An investigation on interior noise reduction using 2d locally resonant phononic crystal with point defect on car ceiling. J Vib Control 25:2
Yang X, Li Y (2013) Topology optimization to minimize the dynamic compliance of a bi-material plate in a thermal environment. Struct Multidisc Optim 47:399–408
Yoon GH, Jensen JS, Sigmund O (2007) Topology optimization of acoustic–structure interaction problems using a mixed finite element formulation. Int J Num Methods Eng 70:1049–1075
Yousaf M, Bujny M, Zurbrugg N, Detwiler D, Duddeck F (2020) Similarity control in topology optimization under static and crash loading scenarios. Eng Optim 53:1523–1538
Zhang Y, Wu H, Jiang W, Kessissoglou N (2017) Acoustic topology optimization of sound power using mapped acoustic radiation modes. Wave Motion 70:90–100
Zhang Z, Zhang Y, Huang C, Liu X (2018) Low-noise structure optimization of a heavy commercial vehicle cab based on approximation model. J Low Frequency Noise Vib Active Control 37:987–1002
Zheng L, Fang Z, Tang Z, Zhan Z (2015) The design optimization of vehicle interior noise through structural modi?cation and constrained layer damping treatment. SAE Technical Paper, 2015-01-0663 https://doi.org/10.4271/2015-01-0663

Publisher's Note Springer Nature remains neutral with regard to jurisdictional claims in published maps and institutional affiliations.

Springer Nature or its licensor (e.g. a society or other partner) holds exclusive rights to this article under a publishing agreement with the author(s) or other rightsholder(s); author self-archiving of the accepted manuscript version of this article is solely governed by the terms of such publishing agreement and applicable law.